JACS
JOURNAL OF THE AMERICAN CHEMICAL SOCIETY
Article
pubs.acs.org/JACS

A Preorganized Ditopic Borane as Highly Efficient One- or Two-Electron Trap

Alexander Hübner,[†] Thomas Kaese,[†] Martin Diefenbach,[†] Burkhard Endeward,[‡] Michael Bolte,[†] Hans-Wolfram Lerner,[†] Max C. Holthausen,*[,†] and Matthias Wagner*[,†]

[†]Institut für Anorganische Chemie, Goethe-Universität Frankfurt, Max-von-Laue-Str. 7, D-60438 Frankfurt am Main, Germany

[‡]Institut für Physikalische und Theoretische Chemie, Goethe-Universität Frankfurt, Max-von-Laue-Str. 7, D-60438 Frankfurt am Main, Germany

Supporting Information

ABSTRACT: Reduction of the bis(9-borafluorenyl)methane **1** with excess lithium furnishes the red dianion salt $Li_2[\mathbf{1}]$. The corresponding dark green monoanion radical $Li[\mathbf{1}]$ is accessible through the comproportionation reaction between **1** and $Li_2[\mathbf{1}]$. EPR spectroscopy on $Li[\mathbf{1}]$ reveals hyperfine coupling of the unpaired electron to two magnetically equivalent boron nuclei ($a(^{11}B)$ = 5.1 ± 0.1 G, $a(^{10}B)$ = 1.7 ± 0.2 G). Further coupling is observed to the unique B−C*H*−B bridgehead proton ($a(^1H)$ = 7.2 ± 0.2 G) and to eight aromatic protons ($a(^1H)$ = 1.4 ± 0.1 G). According to X-ray crystallography, the B···B distances continuously decrease along the sequence **1** → $[\mathbf{1}]^{\bullet-}$ → $[\mathbf{1}]^{2-}$ with values of 2.534(2), 2.166(4), and 1.906(3) Å, respectively. Protonation of $Li_2[\mathbf{1}]$ leads to the cyclic borohydride species $Li[\mathbf{1H}]$ featuring a B−H−B two-electron-three-center bond. This result strongly indicates a nucleophilic character of the boron atoms; the reaction can also be viewed as rare example of the protonation of an element−element σ bond. According to NMR spectroscopy, EPR spectroscopy, and quantum-chemical calculations, $[\mathbf{1}]^{2-}$ represents a closed-shell singlet without any spin contamination. Detailed wave function analyses of $[\mathbf{1}]^{\bullet-}$ and $[\mathbf{1}]^{2-}$ reveal strongly localized interactions of the two boron p_z-type orbitals, with small delocalized contributions of the 9-borafluorenyl π systems. Overall, our results provide evidence for a direct B−B one-electron and two-electron bonding interaction in $[\mathbf{1}]^{\bullet-}$ and $[\mathbf{1}]^{2-}$, respectively.

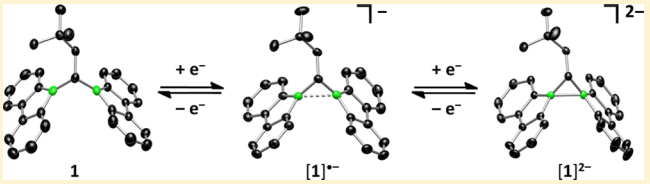

INTRODUCTION

Our groups have recently reported the first structurally characterized compound containing a B·B one-electron-two-center (*1e2c*) σ bond ($[\mathbf{I}]^{\bullet-}$; Figure 1).[1] Key to success was the design of a preorganized ditopic borane **I**,[2] in which an optimal σ overlap of the two empty boron p orbitals offered suitable conditions for the incorporation of the odd electron. The obvious question arising next is to ask: Can we also create a B−B *two*-electron σ bond simply by placing *two* electrons in between a pair of tricoordinate boron atoms?[2] On the one hand, the resulting species $[R_3B{-}BR_3]^{2-}$ would be isoelectronic to common alkanes, on the other hand, the electrostatic repulsion between the two anionic boron centers is expected to destabilize the molecular scaffold. The adverse effect of Coulomb repulsion must indeed be taken seriously, as underscored by the facts that we were so far unable to prepare $[\mathbf{I}]^{2-}$ through further injection of electrons into $[\mathbf{I}]^{\bullet-}$ and that only two examples of $[R_3B{-}BR_3]^{2-}$ anions have been described in the literature so far: (1) Matsuo, Tamao et al. synthesized the dilithium diborane(6) dianion $Li_2[\mathbf{II}]$ through the reduction of the corresponding sterically shielded diborane(6) with lithium naphthalenide (Figure 1).[3] (2) Power et al. isolated small quantities of the dimeric 9*H*-9-borafluorene dianion $[\mathbf{III}]^{2-}$ after they had treated the bulky arylboron dibromide 2,6-$Trip_2C_6H_3BBr_2$ with KC_8 (Trip = 2,4,6-*i*$Pr_3C_6H_2$; Figure 1).[4]

Especially the latter serendipitous finding can be taken as good indication that 9-borafluorene-9-yl may in fact serve as a proper organoboron moiety for the targeted synthesis of $[R_3B{-}BR_3]^{2-}$ species. Our failure to prepare $[\mathbf{I}]^{2-}$ from $[\mathbf{I}]^{\bullet-}$ is thus likely attributable to the choice of the 2,2′-biphenyldiyl backbone, which leads to the conclusion that B−B two-electron and B·B one-electron σ bonds are not necessarily best supported by the same bridging unit. After careful screening of a number of different linkers, we now found that two-electron reduction of the diborylmethane **1**[5] with elemental lithium cleanly furnishes the closed-shell dianion $Li_2[\mathbf{1}]$ (Scheme 1), and herein we report its full characterization. Concerning its reactivity, we will show that treatment of $Li_2[\mathbf{1}]$ with the neutral borane **1** leads to the isolable radical anion $[\mathbf{1}]^{\bullet-}$, whereas the addition of a strong Brønsted acid yields $Li[\mathbf{1H}]$ through protonation of the formal B−B σ bond (Scheme 1). We further report the results of a detailed quantum chemical bonding analysis of **1**, $[\mathbf{1}]^{\bullet-}$, $[\mathbf{1}]^{2-}$, and of the Li-complexed species of the latter two compounds, and comparison is made to the bonding properties of $[\mathbf{I}]^{\bullet-}$ and $[\mathbf{I}]^{2-}$.

Received: February 6, 2015
Published: February 27, 2015

DOI: 10.1021/jacs.5b01192
J. Am. Chem. Soc. 2015, 137, 3705−3714

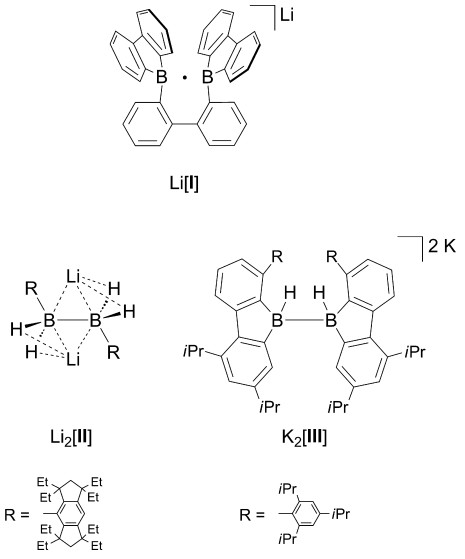

Figure 1. Compound Li[**I**] features a one-electron-two-center bond between two borane moieties, whereas compounds Li_2[**II**] and K_2[**III**] contain two-electron-two-center bonds.

Scheme 1. Two-Electron Reduction of the Diborylmethane 1 to Give Li_2[1]; Comproportionation of 1 and Li_2[1] to Give Li[1]; Synthesis of the B−H−B-Bridged Species Li[1H] through Protonation of Li_2[1] or Hydride Addition to 1[a]

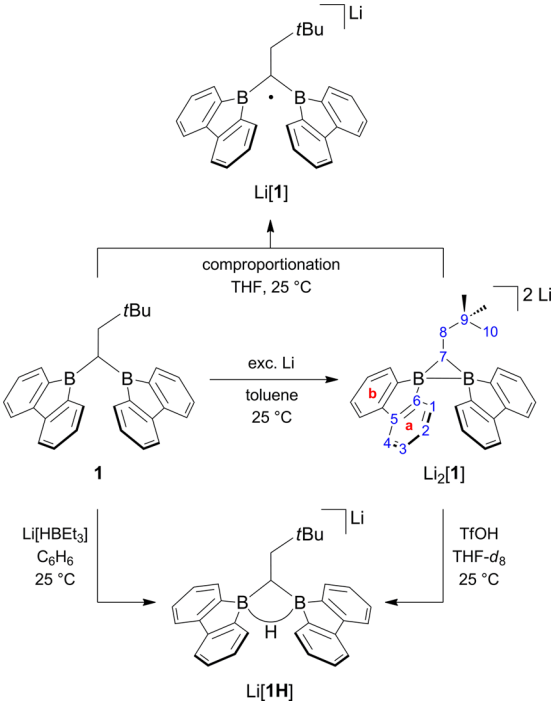

[a]The numbering scheme for the assignment of NMR data is shown using Li_2[**1**] as the example.

RESULTS AND DISCUSSION

In the cyclic voltammogram (CV) the diborylmethane **1** (Scheme 1)[5] undergoes two reversible redox transitions at half-wave potentials of $E_{1/2}$ = −1.76 and −2.17 V (THF, vs FcH/FcH^+; FcH = ferrocene, cf. the Supporting Information (SI) for the CV plot). With $E_{1/2}$ values of −1.49 and −1.75 V the 2,2′-biphenyldiyl-bridged species **I** is easier to reduce under comparable conditions.[1] We suppose that these differences are due to a more efficient σ overlap between the boron p-orbitals in **I** compared to **1**: While **I** possesses a somewhat longer B···B distance (2.920(6) Å)[2] than **1** (2.534(2) Å),[5] the angle between the normals to the two BC_3 planes is only 12.4(2)°[2] in **I** but as large as 74.3(1)°[5] in **1**. Controlled exhaustive reduction of **1** at an electrode potential of E_w = −1.9 V leads to the simultaneous evolution of several new UV−vis absorption bands in a one-electron process (λ_{max} = 357, 432, and 775 nm; Figure 2 top, green curves). If the reduction is

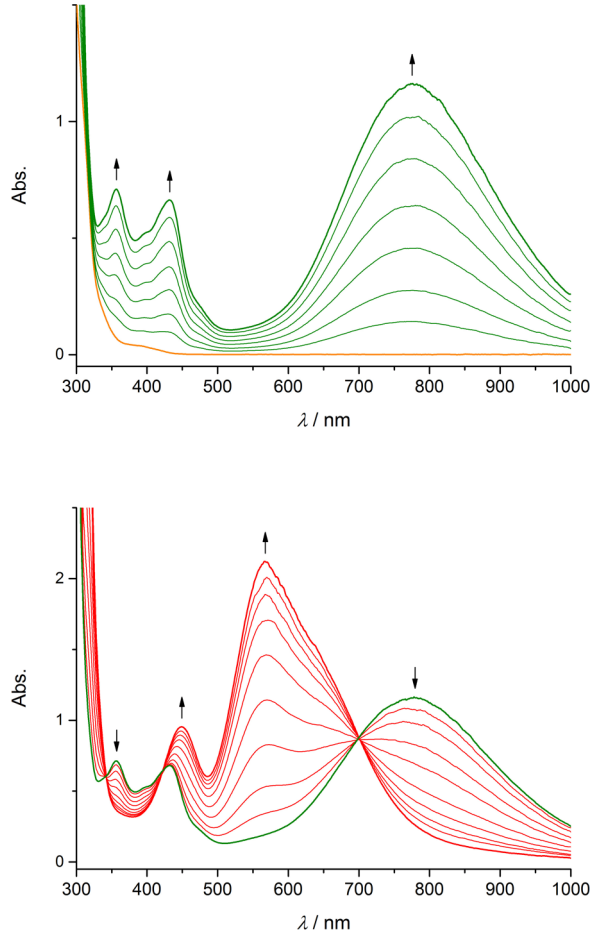

Figure 2. UV−vis absorption spectra were recorded in THF at room temperature during controlled potential electrolysis of **1** at a Pt-net electrode (supporting electrolyte: [nBu$_4$N][PF_6] (0.1 M)). Top: reduction of **1** (orange) to $[\mathbf{1}]^{\bullet-}$ (green) at E_w = −1.9 V. Bottom: subsequent reduction of the electrogenerated $[\mathbf{1}]^{\bullet-}$ (green) to $[\mathbf{1}]^{2-}$ (red) at E_w = −2.4 V.

continued further at a more cathodic potential of E_w = −2.4 V, the absorption bands of the primary reduction product gradually decrease with the concomitant appearance of new absorption bands at λ_{max} = 450 and 568 nm (one-electron process; Figure 2 bottom, red curves). Isosbestic points at λ_{iso} = 342, 423, and 700 nm point toward a clean conversion of $[\mathbf{1}]^{\bullet-}$ to $[\mathbf{1}]^{2-}$ without the formation of intermediates or byproducts. Moreover, at applied potentials of E_w = −1.8 V and E_w = −1.3 V the sample is sequentially taken back to the oxidation state of the neutral diborylmethane **1** (UV−vis spectroscopical control). The observation that **1** and its reduction products are well-behaved under the conditions of spectroelectrochemistry is a strong indication for the accessibility of $[\mathbf{1}]^{\bullet-}$ and

DOI: 10.1021/jacs.5b01192
J. Am. Chem. Soc. 2015, 137, 3705−3714

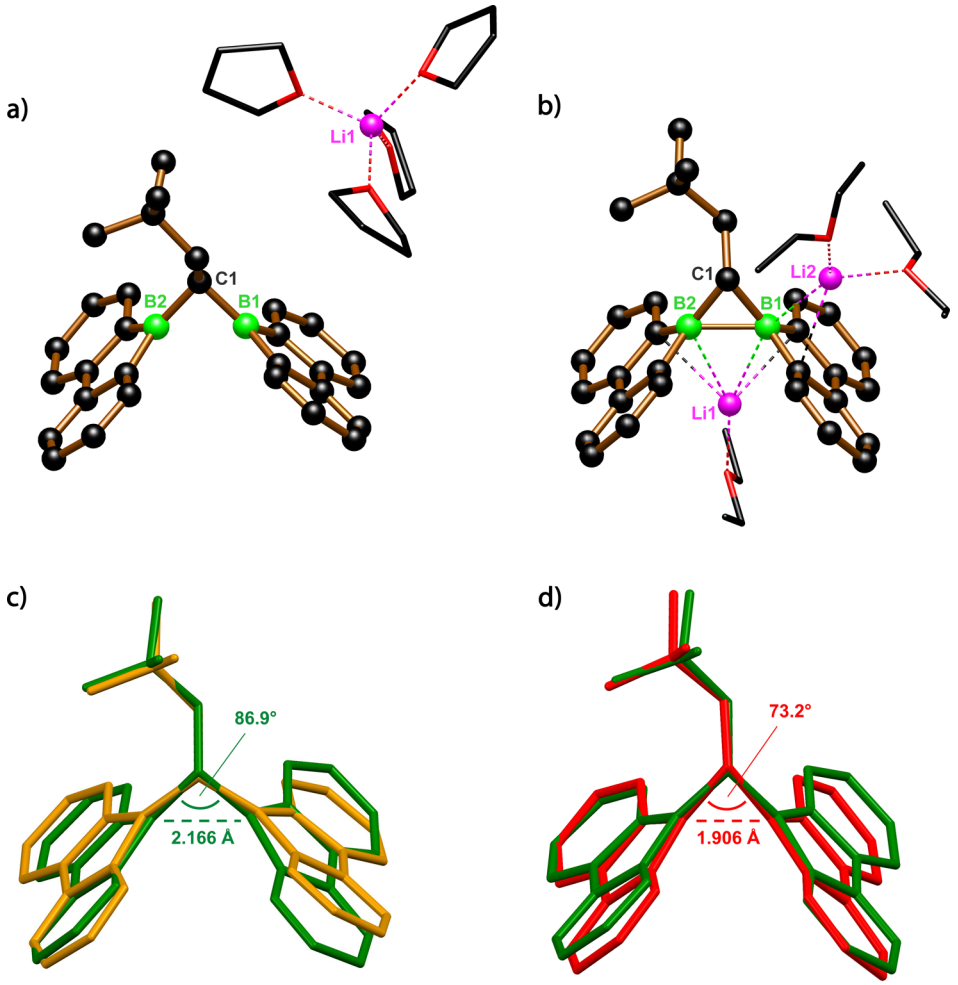

Figure 3. Solid-state structures of (a) $[Li(thf)_4][\mathbf{1}] \times THF$ (cocrystallized THF omitted for clarity) and (b) $[Li(Et_2O)_2][Li(Et_2O)][\mathbf{1}]$. Overlay of the molecular scaffolds of (c) **1** (orange) with $[\mathbf{1}]^{\bullet-}$ (green) and (d) $[\mathbf{1}]^{\bullet-}$ (green) with $[\mathbf{1}]^{2-}$ (red).

$[\mathbf{1}]^{2-}$ on a preparative scale. There is pleasing qualitative agreement between the experimental and the computed UV–vis absorption spectra of the three species **1**, $[\mathbf{1}]^{\bullet-}$, and $[\mathbf{1}]^{2-}$ (see Figure S22 in the SI). Natural transition orbital (NTO) analyses reveal that the dominant features in the computed spectra of the intensely colored anions $[\mathbf{1}]^{\bullet-}$ and $[\mathbf{1}]^{2-}$ originate from charge-transfer transitions (see Table S4 in the SI). The excitations promote a shift of electron density from orbitals strongly localized in the region between the two boron atoms to orbitals located on the borafluorene moieties.

Addition of excess lithium metal to a yellow toluene solution of **1** leads to the precipitation of the red compound $Li_2[\mathbf{1}]$ in yields up to 80% within 14 d (Scheme 1; *note*: the yield is only slightly lower if the product is harvested already after 7 d).[6] Crystals of $[Li(Et_2O)_2][Li(Et_2O)][\mathbf{1}]$ suitable for X-ray diffraction were obtained from Et_2O at room temperature. A comproportionation reaction between equimolar amounts of $Li_2[\mathbf{1}]$ and **1** in THF at room temperature provides clean access to the persistent dark green radical $Li[\mathbf{1}]$. X-ray-quality crystal blocks of $[Li(thf)_4][\mathbf{1}] \times THF$ were grown from a saturated THF/Et_2O solution at −30 °C.

Figure 3a and 3b display the solid-state structures of $[Li(thf)_4][\mathbf{1}] \times THF$ and $[Li(Et_2O)_2][Li(Et_2O)][\mathbf{1}]$, respectively. While the Li^+ ion of $[Li(thf)_4][\mathbf{1}] \times THF$ is fully solvent separated (Figure 3a), both Li^+ ions of $[Li(Et_2O)_2][Li(Et_2O)][\mathbf{1}]$ form close contacts with the $[\mathbf{1}]^{2-}$ anion (Figure 3b): Li(1) binds to only one Et_2O ligand and resides between the two 9-borafluorene-9-yl planes with Li(1)···B(1) and Li(1)···B(2) distances of 2.326(5) and 2.383(5) Å, respectively. The shortest Li(1)···C contacts are shown as dashed lines and amount to 2.464(6) and 2.496(6) Å. Li(2) carries two Et_2O ligands; its coordination sphere is completed by B(1) (2.328(4) Å) and one carbon atom (2.462(4) Å). Figure 3c and 3d show overlays of the molecular scaffolds of **1** (orange) with $[\mathbf{1}]^{\bullet-}$ (green) and $[\mathbf{1}]^{\bullet-}$ (green) with $[\mathbf{1}]^{2-}$ (red). We observe a gradual contraction of the B(1)···B(2) distance along the sequence **1** (2.534(2) Å) → $[\mathbf{1}]^{\bullet-}$ (2.166(4) Å) → $[\mathbf{1}]^{2-}$ (1.906(3) Å) with differences of 0.37 and 0.26 Å, respectively (Table 1). This contraction is accompanied by a continuous compression of the B(1)–C(1)–B(2) angle from 105.5(2)° (**1**) to 86.9(2)° ($[\mathbf{1}]^{\bullet-}$), and finally to 73.2(1)° ($[\mathbf{1}]^{2-}$; Table 1).

The B(1)···B(2) distance in $[\mathbf{1}]^{\bullet-}$ is shorter by 0.099 Å than the corresponding B·B *1e2c* bond in $[\mathbf{I}]^{\bullet-}$ (2.265(4) Å; Table 1). In $[\mathbf{1}]^{2-}$, the B(1)···B(2) distance is comparable to that in $[\mathbf{II}]^{2-}$ (1.924(3) Å), and longer than the B···B distance in $[\mathbf{III}]^{2-}$ (1.83(2) Å). Another parameter of interest is the degree of boron pyramidalization. As a quantitative measure, we take the angle θ at which the exocyclic B–C bond vector intersects the endocyclic BCC plane. In a trigonal-planar boron environment θ equals 180°, whereas θ = 125.3° signifies a tetrahedral situation. Both in $[\mathbf{1}]^{\bullet-}$ and in $[\mathbf{1}]^{2-}$, the boron

DOI: 10.1021/jacs.5b01192
J. Am. Chem. Soc. 2015, 137, 3705–3714

Table 1. Comparison of Key Structural Parameters of 1,[5] $[\mathbf{1}]^{\bullet-}$, $[\mathbf{1}]^{2-}$, $[\mathbf{1H}]^{-}$, I,[2] $[\mathbf{I}]^{\bullet-}$,[1] and $[\mathbf{I}]^{2-}$ According to X-ray Crystallography and DFT Calculations[a]

	B(1)···B(2)/Å		B(1)−C(1)−B(2)/°		θ_{av}/°	
compound	X-ray	calcd	X-ray	calcd	X-ray	calcd
1	2.534(2)	2.376	105.5(2)	98.7	178.5	176.4
$[\mathbf{1}]^{\bullet-}$	2.166(4)	2.129	86.9(2)	85.2	174.0	177.6
		2.126		*85.2*		*174.8*
$[\mathbf{1}]^{2-}$	1.906(3)	1.878	73.2(1)	72.4	168.4	167.4
		1.948		*75.9*		*167.0*
$[\mathbf{1H}]^{-}$	1.954(5)	1.901	75.4(2)	72.8	150.8	148.4
		1.908		*73.3*		*143.4*
I	2.920(6)	2.894	–	174.9	177.0	174.9
$[\mathbf{I}]^{\bullet-}$	2.265(4)	*2.251*	–	*157.3*	156.1	*157.3*
$[\mathbf{I}]^{2-}$	–	*1.889*	–	*141.0*	–	*141.0*

[a]Experimental and DFT metrics given refer to the Li-complexes; computed data for the bare, Li^+-free species are shown in italics.

atoms remain essentially planar with mean values θ_{av} of 174.0° and 168.4°, respectively (Table 1). All experimentally determined key structural parameters are coherent with the computed molecular structures of $[Li(thf)_4][\mathbf{1}]$ and $[Li(Et_2O)_2][Li(Et_2O)][\mathbf{1}]$ (cf. the SI for full details).

An EPR spectrum confirming the open-shell electronic structure of $[\mathbf{1}]^{\bullet-}$ was recorded in THF at room temperature (Figure 4a). Using the hyperfine coupling constants predicted for this species at the PBE0D/EPR-III/COSMO(THF) level as initial guesses (mean DFT-derived values for the two boron nuclei: $a(^{11}B)$ = 5.8 G, $a(^{10}B)$ = 1.9 G), the observed spectrum was finally simulated by assuming hyperfine coupling of the unpaired electron (g_{iso} = 1.998 ± 0.001) to two magnetically equivalent boron nuclei with isotropic coupling constants of $a(^{11}B)$ = 5.1 ± 0.1 G and $a(^{10}B)$ = 1.7 ± 0.2 G. We further assumed coupling to one proton with $a(^1H)$ = 7.2 ± 0.2 G and eight magnetically equivalent protons with $a(^1H)$ = 1.4 ± 0.1 G.

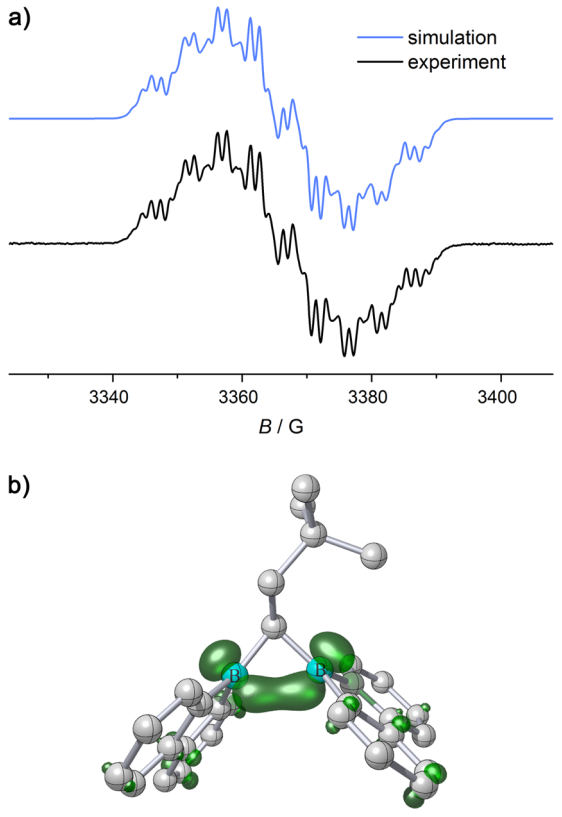

Figure 4. (a) EPR spectrum of the radical anion $[\mathbf{1}]^{\bullet-}$ in THF (experimental spectrum at room temperature (black), simulation fit (blue)). (b) Computed spin density distribution of $[\mathbf{1}]^{\bullet-}$ at an isovalue of 0.0075 a_0^{-3} (green; PBE0D/EPR-III level).

The larger $a(^1H)$ coupling constant can reasonably be assigned to the unique B−C*H*−B bridgehead hydrogen atom (DFT-derived value $a(^1H)$ = 8.0 G). In line with basic mesomeric structure considerations, the spin-density plot of $[\mathbf{1}]^{\bullet-}$ (Figure 4b) indicates that the smaller $a(^1H)$ coupling constant is likely due to the four *ortho* and the four *para* 9-borafluorenyl protons. Both $a(^{11}B)$ and $a(^{10}B)$ values of $[\mathbf{1}]^{\bullet-}$ are close to those reported for $[\mathbf{I}]^{\bullet-}$ (seven-line spectrum; $a(^{11}B)$ = 4.8 ± 0.1 G, $a(^{10}B)$ = 1.6 ± 0.1 G).[1] Moreover, the small value of $a(^{11}B)$ in $[\mathbf{1}]^{\bullet-}$ and the low degree of boron pyramidalization in its solid-state structure provides strong evidence that each boron atom essentially contributes a p_z orbital to the molecule's SOMO (cf. Figure 7a) akin to the situation found for $[\mathbf{I}]^{\bullet-}$. In stark contrast to $[\mathbf{I}]^{\bullet-}$, however, the observed coupling to 9-borafluorenyl protons in $[\mathbf{1}]^{\bullet-}$ indicates that the unpaired electron is no longer exclusively trapped between the two boron atoms, but that spin-density is delocalized to a certain extent within the π-electron systems. We will return to the electronic structure of $[\mathbf{1}]^{\bullet-}$ in considerable detail further below.

In line with a singlet electron configuration, $Li_2[\mathbf{1}]$ is EPR silent in THF solution and gives perfectly well resolved NMR spectra with chemical shift values in ranges typical of diamagnetic species (THF-d_8). This spin-state characterization is further corroborated by the fact that NMR shifts computed for the closed-shell singlet ground state of the bare (i.e., Li^+-free) dianion $[\mathbf{1}]^{2-}$ are in reasonable qualitative agreement with the experimental data (cf. the SI for more details). The ^{7}Li NMR spectrum contains one single resonance at −1.2 ppm, assignable to the $[Li(thf)_4]^+$ solvate complex,[7] which indicates that Li(1) no longer occupies a B−B-bridging position. The ^{11}B resonance of $Li_2[\mathbf{1}]$ appears at −6.7 ppm, thereby testifying to the presence of tetracoordinate boron nuclei;[8] for comparison, $K_2[\mathbf{III}]$ gives rise to an ^{11}B NMR signal at −7.0 ppm (C_6D_6).[4] In contrast to the neutral starting material **1**, which exhibits only one set of ^{1}H or $^{13}C\{^1H\}$ resonances, two sets of signals with equal ratios are observed for the aromatic rings of $Li_2[\mathbf{1}]$, both in the ^{1}H and in the $^{13}C\{^1H\}$ NMR spectrum (cf. the SI for plots of the spectra). The conformational flexibility of $Li_2[\mathbf{1}]$ thus appears to be more restricted than in the neutral starting material.

All key structural and spectroscopic parameters of $[\mathbf{1}]^{\bullet-}$ and $[\mathbf{1}]^{2-}$ are consistent with a predominant accumulation of negative charge density in the space amid B(1) and B(2): (i) If the excess electrons were mainly delocalized over the 9-borafluorenyl π systems, one would expect a more symmetric coordination of the Li^+ ions to the two BC_4 rings of $[Li(Et_2O)_2][Li(Et_2O)][\mathbf{1}]$. (ii) X-ray crystallography reveals a pronounced contraction of the B(1)···B(2) distances along the sequence **1** → $Li[\mathbf{1}]$ → $Li_2[\mathbf{1}]$. Since this trend is quantitatively reproduced by quantum-chemical calculations on the bare anions $[\mathbf{1}]^{\bullet-}$ (2.126 Å) and $[\mathbf{1}]^{2-}$ (1.948 Å), the short B(1)···B(2) distance in $Li_2[\mathbf{1}]$ is clearly not the result of attractive electrostatic interactions within the B···Li···B moiety (cf. the SI for full details). (iii) The lack of conformational flexibility of

DOI: 10.1021/jacs.5b01192
J. Am. Chem. Soc. 2015, 137, 3705−3714

$Li_2[\mathbf{1}]$ in solution together with the absence of B−B bridging Li^+ ions, as revealed by NMR spectroscopy, can straightforwardly be explained assuming the presence of a covalent B(1)−B(2) two-electron-two-center (*2e2c*) bond.

In order to experimentally validate the postulate of a B(1)−B(2) bond by protonation of the accumulated negative charge density, we treated a solution of $Li_2[\mathbf{1}]$ in THF-d_8 with trifluoromethanesulfonic acid (TfOH) and indeed proved the formation of the B−H−B-bridged species Li[**1H**] by NMR spectroscopy (Scheme 1; cf. the SI for more details). To obtain an authentic sample, Li[**1H**] was also synthesized on a preparative scale from **1** and $Li[HBEt_3]$ in C_6H_6 (Scheme 1); single crystals of $[Li(thf)_4][\mathbf{1H}]$ formed from C_6H_6 in the presence of small amounts of THF (Figure 5). The newly

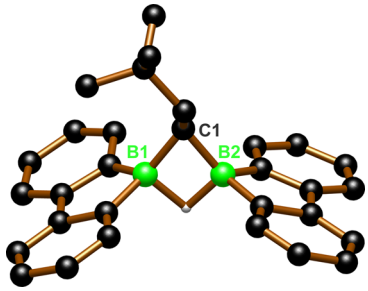

Figure 5. Solid-state structure of $[Li(thf)_4][\mathbf{1H}]$ (solvent separated $[Li(thf)_4]^+$ omitted for clarity).

introduced hydrogen atom gives rise to an extremely broad resonance at 1.83 ppm in the ^1H NMR spectrum (THF-d_8). Similar to $Li_2[\mathbf{1}]$, both the ^1H and the $^{13}C\{^1H\}$ NMR spectrum of Li[**1H**] reveal two sets of aryl resonances. This recurring feature supports our previous assumption that a linking of B(1) and B(2) reduces the average symmetry of the bis(9-borafluorenyl)methane skeleton in solution. With respect to the molecular structures of $[Li(Et_2O)_2][Li(Et_2O)][\mathbf{1}]$ and $[Li(thf)_4][\mathbf{1H}]$ we note a moderate expansion of the B(1)···B(2) distance from 1.906(3) to 1.954(5) Å. The average degree of boron pyramidalization, however, is substantially more pronounced in the latter molecule (θ_{av} = 150.8°) than in the former (θ_{av} = 168.4°; Table 1).

The successful transformation of $Li_2[\mathbf{1}]$ into Li[**1H**] is remarkable for several aspects: (i) We obtain the same result when we add a hydride ion to **1** as when we first inject two electrons and supply the accompanying atomic nucleus at a later stage. (ii) Judging from the experimental evidence gathered so far, $[\mathbf{1}]^{2-}$ belongs to the class of $[R_3B{-}BR_3]^{2-}$ dianions. Its reaction with TfOH represents a very rare example of the successful protonation of an element−element σ bond to furnish an E−H−E two-electron-three-center (*2e3c*) bond.[9] (iii) Taking together the apparent Brønsted basicity of the boron atoms in $[\mathbf{1}]^{2-}$ and the well-known α-acidity of alkylboranes,[10] an (intramolecular) proton shift could conceivably lead to the corresponding borata-alkene/hydridoborate isomer (Figure 6; BR_2 = 9-borafluorenyl, R′ = $CH_2C(CH_3)_3$). Yet, pursuant to the fact that we never observed any indications of the rearranged product in the experiments, the quantum-chemical assessment of such a process in $[\mathbf{1}]^{2-}$ reveals that the rearrangement is endergonic by ΔG^{298} = 12.6 kcal mol^{-1} and kinetically hindered by a significant barrier of 33.1 kcal mol^{-1}. Remarkably, a reversed isomer stability is computed for the parent diboracyclopropane dianion (R = R′ = H), but an even

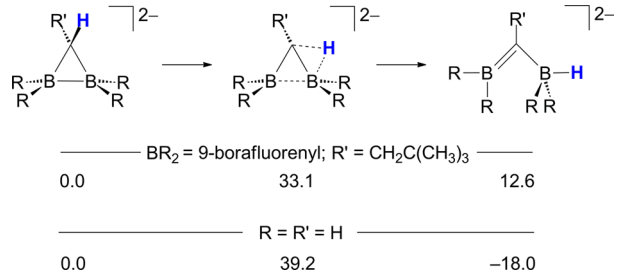

Figure 6. Relative Gibbs energies in kcal mol^{-1} (PBE0D/TZVP) of diboracyclopropane dianions compared to their borata-alkene/hydridoborate isomers for the real system (BR_2 = 9-borafluorenyl, R′ = $CH_2C(CH_3)_3$) and the parent model system (R = R′ = H) together with interconnecting transition states.

higher kinetic barrier is predicted for this model system. (iv) The Li^+ ion is the heavier homologue of the proton. Thus, at first glance the B−H−B bridge in $[Li(thf)_4][\mathbf{1H}]$ and the B···Li···B bridge in $[Li(Et_2O)_2][Li(Et_2O)][\mathbf{1}]$ appear closely related. However, while a QTAIM topological electron density analysis clearly reveals the expected characteristics for covalent B−H−B bond paths in $[\mathbf{1H}]^-$ (see below), the corresponding analyses for any of the Li-coordinated species studied indicate a fundamentally different bonding situation (cf. the SI).

We performed a detailed quantum chemical investigation to gain further insight into the electronic structures of the species under study. To this end, we first verified the suitability of the PBE0D functional to properly assess a potential singlet biradical character of the dianion's wave function by careful comparison of broken-symmetry DFT and MRCI results obtained for the diboracyclopropane model systems $[cyc\text{-}CH_2B_2H_4]^{\bullet-/2-}$ (cf. Figure 6) and the all-carbon analog cyclopropane, $cyc\text{-}C_3H_6$. While the details of this study are provided as Supporting Information, suffice it here to state that the results inspire full confidence in the PBE0D approach and that the ground-state wave functions of all dianionic species discussed in the following represent closed-shell singlet situations without any spin contamination.

We first note that the key frontier molecular orbitals, i.e., the LUMO in **1**, the SOMO in $[\mathbf{1}]^{\bullet-}$, and the HOMO in $[\mathbf{1}]^{2-}$, are dominated by the strongly localized interaction of the two boron p_z-type orbitals, with small delocalized contributions of the borafluorene π systems visible (Figure 7a). As a result of the methylene-bridge enforced orientation of the 9-borafluorenyl moieties the boron p_z orbitals are obviously only poorly aligned. Because of the increasingly closer B−B contact arising upon successive injection of electrons, the orbital interaction is gradually improved in the SOMO of $[\mathbf{1}]^{\bullet-}$ and in the HOMO of $[\mathbf{1}]^{2-}$, but still overlap appears not ideally suited for the formation of a σ bond in both cases.

Evidence for a direct B−B bonding interaction in $[\mathbf{1}]^{\bullet-}$ and $[\mathbf{1}]^{2-}$ was also found among the natural localized molecular orbitals (NLMOs) resulting from a natural bond orbital (NBO) analysis (Figure 7b). For both molecules the corresponding B−B bonding NLMOs involve contributions arising from interaction of the boron atomic orbitals, augmented by a significant participation of orbitals at an adjacent carbon atom of one of the borafluorene rings. In the realm of NBO theory such a semilocalized nature of NLMOs reflects the presence of a physically relevant delocalization of an electron pair (or a single electron in the radical case[11,12]) in the sense of deviations from the representability of the wave function as a set of

DOI: 10.1021/jacs.5b01192
J. Am. Chem. Soc. 2015, 137, 3705−3714

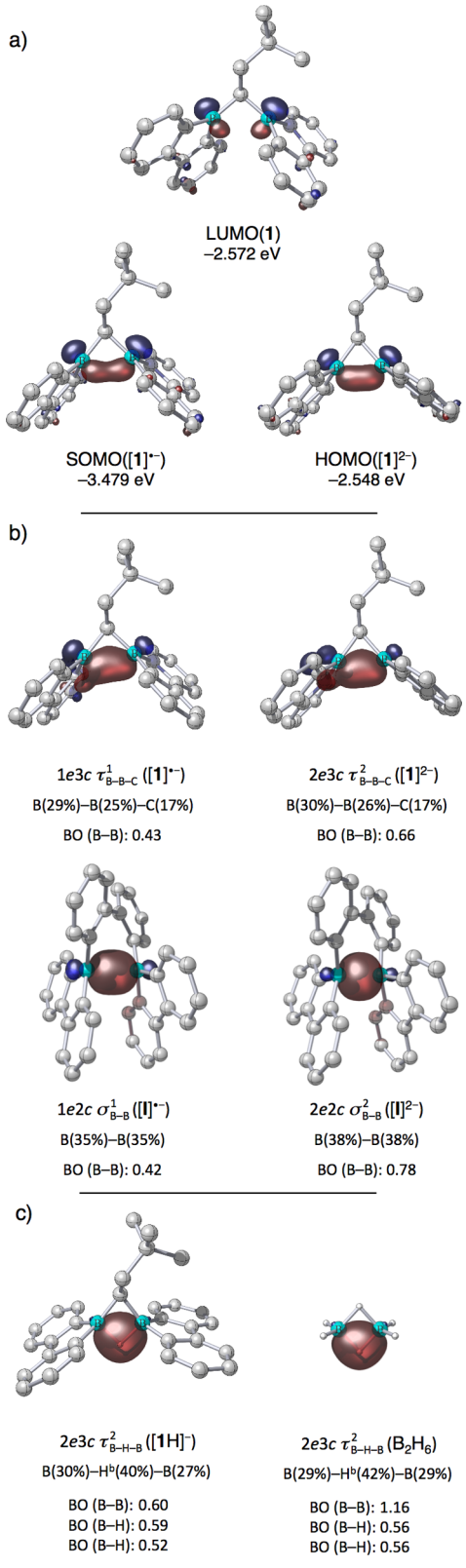

Figure 7. (a) Selected molecular orbitals for the Li^+-free species **1**, $[\mathbf{1}]^{\bullet-}$, and $[\mathbf{1}]^{2-}$. (b) Selected NLMOs for the Li^+-free species $[\mathbf{1}]^{\bullet-}$, $[\mathbf{1}]^{2-}$, $[\mathbf{I}]^{\bullet-}$, and $[\mathbf{I}]^{2-}$. (c) Selected NLMOs for $[\mathbf{1H}]^-$ and B_2H_6. NLMO occupancies, dominantly contributing NAOs, and NLMO/NPA bond orders (BO) are given. Results are based on PBE0D/TZVP wave functions and isosurfaces are plotted at an isovalue of 0.075 $a_0^{-3/2}$; carbon-bonded H atoms omitted for clarity.

localized one-center and two-center NBOs, which serve as a conveniently interpretable basis of a *natural Lewis structure*.[13] Correspondingly, the nature of both NLMOs is characterized by the NBO analysis as a one-electron- and two-electron-three-center B–B bonding situation, respectively. In other words, a Lewis-like description of the boron–boron bonding interaction would involve further resonance structures in addition to the representation as a one-electron bond between the boron atoms in $[\mathbf{1}]^{\bullet-}$ or a two-electron bond between the boron atoms in $[\mathbf{1}]^{2-}$. This contrasts the B–B bonding situation in $[\mathbf{I}]^{\bullet-}$ and $[\mathbf{I}]^{2-}$ displayed for comparison in Figure 7b: for both species the NBO analysis reveals substantially more localized NLMOs, clearly characterized as *1e2c* and *2e2c* B–B bonding situations, respectively. Notwithstanding these qualitative differences, the computed NLMO/NPA bond orders[14] are almost identical for $[\mathbf{1}]^{\bullet-}$ and $[\mathbf{I}]^{\bullet-}$, whereas those for $[\mathbf{1}]^{2-}$ and $[\mathbf{I}]^{2-}$ indicate a slightly stronger B–B bonding interaction in the latter (NPA: natural population analysis; Figure 7). Overall, the NBO picture of a more delocalized B–B single-electron bond in $[\mathbf{1}]^{\bullet-}$ as compared to $[\mathbf{I}]^{\bullet-}$ is reflected as well in the computed spin-density distributions for both species (cf. Figure 4 and ref 1) and is in line with the EPR results discussed above. With bond orders of 0.66 and 0.78 the B–B bonding interactions in $[\mathbf{1}]^{2-}$ and $[\mathbf{I}]^{2-}$ are characterized as moderately weak, comparable to the direct B–B bond order of 0.60 present in the B–H–B bridged species $[\mathbf{1H}]^-$ (Figure 7c). The B–H–B hydride bridge in the latter species represents, according to the NBO analysis, a genuine *2e3c* bonding situation. The corresponding NLMO is shown in Figure 7c and comparison with one of the two corresponding NLMOs in diborane reveals almost identical characteristics in terms of natural atomic orbital (NAO) composition of the three contributing atomic centers as well as B–H–B NLMO/NPA bond orders.

A B–B bonding interaction in compounds $[\mathbf{1}]^{\bullet-}$ and $[\mathbf{1}]^{2-}$ is indicated by both, the structural B–B distance metrics as well as the orbital analyses. Yet, topological analyses of the computed electron densities according to Bader's quantum theory of atoms in molecules (QTAIM) revealed no B–B bond path in either molecule. This result is surprising in view of the marked similarities between the orbital-analysis results for both species and those obtained for $[\mathbf{I}]^{\bullet-}$ and $[\mathbf{I}]^{2-}$ and the fact that the NBO bonding picture for the latter two species is consistently complemented by the finding of B–B bond paths[1] with bond-critical-point (bcp) characteristics revealing covalent bonding interactions between the QTAIM boron atomic basins.

Bader has clearly stressed that a bond path must not be understood as representing a bond.[15] Rather, the concept of a *chemical bond* linking atoms is replaced within QTAIM by the concept of *chemical bonding*, which is indicated by a shared interatomic surface between atomic basins, the presence of an associated bond path ("a line of maximum electron density that denotes that the atoms it links are bonded to one another"[16]), and a bond-critical point located at the minimum of electron density along the bond path where the density gradient vanishes. For a system at equilibrium geometry[17] the network of bond paths, the molecular graph, represents the molecular structure in terms of pairwise chemical bonding interactions among atoms as a consequence of electronic charge density accumulated between them. A vast body of investigations on molecular graphs illustrates that in most of the cases a bond path exists where, intuitively, a chemical bond is expected, although the (common) finding of chemically unexpected bond

DOI: 10.1021/jacs.5b01192
J. Am. Chem. Soc. 2015, 137, 3705–3714

paths has led to controversial discussions regarding the validity of the conceptual connection between a bond path and interatomic bonding.[16,18−24] Precedence for the opposite situation, that is, the absence of a bond path where a chemical bond is expected, also exists, and a number of experimental and theoretical charge-density studies have investigated difficulties in assessing the nature of bonding interactions by means of QTAIM.[25−33] Further analysis of the QTAIM results for $[\mathbf{1}]^{\bullet-}$ and $[\mathbf{1}]^{2-}$ reveals that the respective atomic basins of the bridging carbon atoms extend between those of the boron atoms in both cases. Correspondingly, the gradient vector field plots in Figure 8 illustrate the lack of shared boron−boron

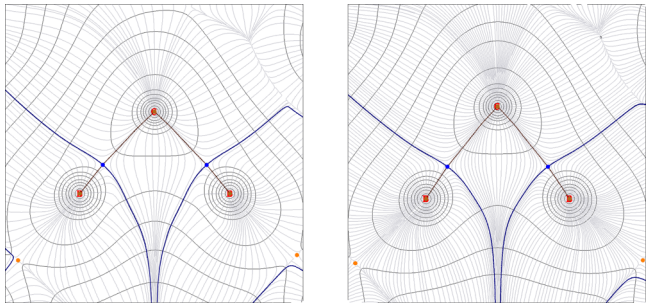

Figure 8. Plot of the gradient vector field of ρ for $[\mathbf{1}]^{\bullet-}$ (left) and $[\mathbf{1}]^{2-}$ (right) in the central B−C−B plane; bond paths are shown in red, zero-flux surfaces and B−C bond critical points (circles) in blue.

interatomic surfaces. This topological feature in the density distribution ρ clearly excludes the presence of B−B bond paths. We note, however, that the charge densities in the regions between the boron atoms are rather low (e.g., ρ = 0.075 and 0.09 au at the midpoint between the boron atoms in $[\mathbf{1}]^{\bullet-}$ and $[\mathbf{1}]^{2-}$, respectively) and exhibit a rather flat topology.

In the light of earlier studies emphasizing the dependence of the charge density topology on the theoretical level[33,34] we investigated the dianion $[\mathbf{1}]^{2-}$ together with the diboracyclopropane dianion model system (cf. Figure 6; R = R′ = H) in some more detail. The QTAIM analysis at the gas phase equilibrium structure of the diboracyclopropane dianion model disclosed a B−B bond path and, with negative values of the Laplacian and the total energy density, the bcp properties indicate a covalent bonding interaction (cf. the SI for details). However, the associated ring-critical point (rcp) is located merely 0.08 Å apart and both reside in a very flat density region (ρ_{bcp} = 0.15 au, ρ_{rcp} = 0.14 au).[35] This situation indicates a topologically unstable molecular structure close to a catastrophe point.[36] As a characteristic of such topologies, subtle changes in the density (caused, e.g., by small changes of the nuclear coordinates) often lead to a collapse of the rcp into the bcp; both critical points will thereby vanish, which causes an abrupt change in the molecular graph. Accordingly, we found no B−B bond path in the partially optimized model system with fixed coordinates of the BCB ring atoms taken from the optimized structure of $[\mathbf{1}]^{2-}$. For the full system $[\mathbf{1}]^{2-}$, artificial compression of the B−B distance during a relaxed scan actually evokes a B−B bond path and a bcp, but only at a B−B distance below 1.6 Å. Because this compression is associated with an increase in total energy by 18 kcal mol^{-1}, this point is clearly not accessible assuming a thermally feasible displacement along the low B−C−B bending vibrational mode in $[\mathbf{1}]^{2-}$ ($\tilde{\nu}$ = 185 cm^{-1}). This excludes the relevant supposition of a dynamic occurrence of a B−B bond path in $[\mathbf{1}]^{2-}$ in the sense of judicious discussions on the influence of nuclear vibrational motions on the charge density topology.[27,37]

Hence at this point we are left to conclude that there is no chemical bonding between the boron atoms in $[\mathbf{1}]^{\bullet-}$ or in $[\mathbf{1}]^{2-}$ within Bader's definition.[17] We have gathered information indicating that the nuclear configurations of the central B−C−B moieties in $[\mathbf{1}]^{\bullet-}$ and $[\mathbf{1}]^{2-}$ give rise to topologically unstable charge density characteristics. Apart from potential problems related to the pronouncedly diffuse and flat character of the excess electron density in the anions $[\mathbf{1}]^{\bullet-}$ and $[\mathbf{1}]^{2-}$, there is growing evidence in the available pertinent literature that triangular nuclear arrangements generally tend to provoke topological instabilities,[29] which might in fact explain reported QTAIM failings to identify expected bond paths.[25−33] Correspondingly, the QTAIM analysis of $[\mathbf{1H}]^{-}$ with its *four-membered* central ring smoothly unveils bonding interactions typical for a B−H−B *2e3c* bridge, with curved bond paths and bcp characteristics closely resembling those of the bcps in parent B_2H_6 (Figure 9).

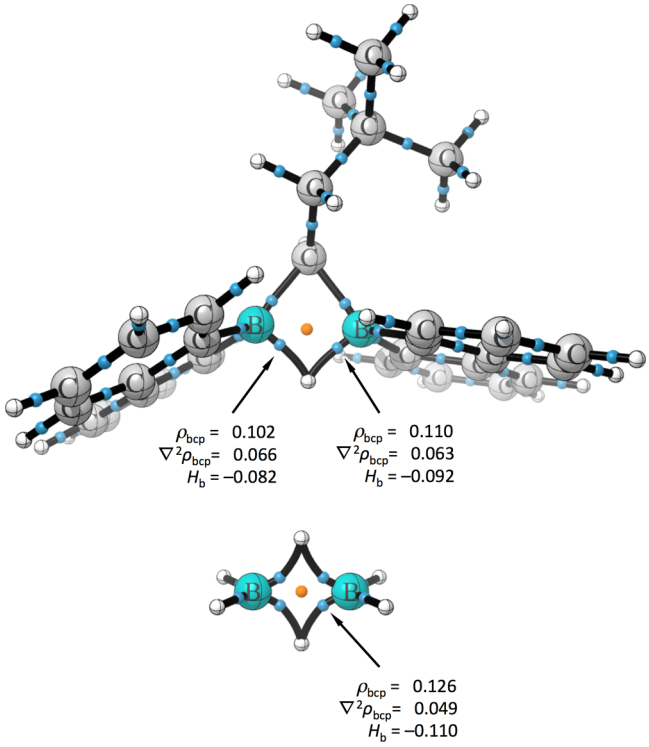

Figure 9. Molecular graphs for $[\mathbf{1H}]^{-}$ and B_2H_6 together with bcp properties for the B−H−B bridges (electron density ρ in $e\ a_0^{-3}$, Laplacian $\nabla^2\rho$ in $e\ a_0^{-5}$, total energy density H_b in $E_h\ a_0^{-3}$); bond paths are shown as black lines, bcps as blue spheres, and rcps as orange spheres.

CONCLUSION

In the present contribution we have shown that one and also two electrons can be trapped amid two three-coordinate boron atoms, provided they are properly preorganized within suitable organoborane scaffolds. The injected electron density has pronounced consequences for key structural features. First and foremost, the B−C−B bond angle becomes more acute, and the B−B distance decreases, along the sequence from the neutral diborylmethane **1** via the anion radical $[\mathbf{1}]^{\bullet-}$ to the closed-shell dianion $[\mathbf{1}]^{2-}$. At first glance this indicates the presence of

DOI: 10.1021/jacs.5b01192
J. Am. Chem. Soc. 2015, 137, 3705−3714

covalent bonding interactions, insinuating the formation of *1e2c* and *2e2c* bonds, respectively, among the formerly electron-deficient boron atoms. Such an interpretation inherently rests upon the assumption that the added charge density is largely localized in the void space between the boron atoms, and indeed, we were able to map it by subsequent introduction of a proton, yielding the hydride-bridged B−H−B species $[\mathbf{1H}]^-$. Before this clear-cut experimental background, the lack of a bond path between the boron atoms in either species, $[\mathbf{1}]^{\bullet-}$ and $[\mathbf{1}]^{2-}$, is intriguing, as this is one of the most relied-upon criteria that theory can provide to identify interatomic bonding interactions. Analyses within the NBO framework, in turn, provide a well-defined basis for the interpretation of our experimental findings and fully support the view of covalent B−B bonding. Striking discrepancies resulting from the application of NBO theory and QTAIM, both widely used quantum-chemical tools, to interpret one and the same molecular charge density have been observed earlier. These problems appear to be particularly notorious for topologically unstable three-membered ring systems, in which the collapse of ring-critical and bond-critical points can lead to unexpected disappearance of a bond path.[28]

EXPERIMENTAL SECTION

General Considerations. All reactions and manipulations were carried out in an argon-filled glovebox or by applying standard Schlenk techniques under an argon atmosphere. C_6H_6/C_6D_6, toluene, and THF/THF-d_8 were dried over Na/K alloy *without* benzophenone (2−3 d). Prior to use, the solvents were distilled from the drying agent and degassed by applying four freeze−pump−thaw cycles. Compound **1** was synthesized according to a literature procedure.[5]

NMR: Avance 300, Avance 400, Avance III 500 HD. Chemical shifts are referenced to (residual) solvent signals (^{1}H/^{13}C{^{1}H}; C_6D_6: δ = 7.16/128.06 ppm; THF-d_8: δ = 3.58/67.21 ppm) or external aqueous LiCl (^{7}Li), $BF_3{\cdot}Et_2O$ (^{11}B; ^{11}B{^{1}H}), and $Si(CH_3)_4$ (^{29}Si INEPT). Abbreviations: s = singlet, d = doublet, t = triplet, vt = virtual triplet, m = multiplet, n. r. = multiplet expected in the NMR spectrum but not resolved, n. o. = not observed. Cyclic voltammograms were recorded at room temperature using an EG&G Princeton Applied Research 263A potentiostat with a platinum disk working electrode (diameter 2.00 mm). The reference electrode was a silver wire on which AgCl had been deposited by immersing the wire into HCl/HNO_3 (3:1). [nBu$_4$N][PF_6] (0.1 M) was employed as the supporting electrolyte. All potential values are referenced against the FcH/FcH$^+$ couple ($E_{1/2}$ = 0 V). Coulometric measurements were performed at room temperature using a Pt-net electrode. EPR spectra were recorded with a Bruker Elexsys E500 CW EPR spectrometer at X-band frequencies in a TE 102 cavity and at room temperature. EPR simulations were done using the SimFonia software of Bruker. Combustion analyses were performed by the Microanalytical Laboratory of the Goethe-University Frankfurt or by the Microanalytical Laboratory Pascher (Remagen, Germany).

Synthesis of Li_2[1]. Lithium granules (120 mg, 17.3 mmol) were manually divided into small pieces and added at room temperature to a yellow solution of **1** (100 mg, 0.244 mmol) in toluene (20 mL). The reaction mixture was stirred for 14 d, whereupon its color changed to red and a deep red precipitate formed. The suspension was separated from unreacted lithium granules via syringe, the red precipitate of $Li_2[\mathbf{1}]$ was collected on a frit and dried under vacuum. Yield: 78 mg (0.19 mmol, 78%). Red crystals of $[Li(Et_2O)_2][Li(Et_2O)][\mathbf{1}]$ suitable for X-ray crystallography were obtained from an Et_2O solution by slow evaporation of the solvent at room temperature. ^{1}H NMR (400.1 MHz, THF-d_8, 298 K) δ = 8.20 (d, ^3J(H,H) = 7.6 Hz, 2H; H-1a), 7.98 (d, ^3J(H,H) = 7.5 Hz, 2H; H-1b), 7.59 (d, ^3J(H,H) = 7.6 Hz, 2H; H-4a), 7.57 (d, ^3J(H,H) = 7.5 Hz, 2H; H-4b), 6.92−6.86 (m, 4H; H-2a,2b), 6.65 (dvt, ^4J(H,H) = 1.0 Hz, 2H; H-3a), 6.64 (dvt, ^4J(H,H) = 1.1 Hz, 2H; H-3b), 2.41 (d, ^3J(H,H) = 7.4 Hz, 2H; H-8), 2.05 (t, ^3J(H,H) = 7.4 Hz, 1H; H-7), 0.78 (s, 9H; H-10); ^{7}Li NMR (116.6 MHz, THF-d_8, 298 K) δ = −1.2 ($h_{1/2}$ = 80 Hz); ^{11}B NMR (128.4 MHz, THF-d_8, 298 K) δ = −6.7 ($h_{1/2}$ = 270 Hz); ^{13}C{^{1}H} NMR (100.6 MHz, THF-d_8, 298 K) δ = 162.2* (C-6b), 161.0* (C-6a), 143.6 (C-5a), 143.1 (C-5b), 131.1 (C-1a), 129.0 (C-1b), 121.5, 121.4 (C-2a,2b), 118.3, 118.2 (C-4a,4b), 117.6 (C-3b), 117.4 (C-3a), 45.6 (C-8), 33.2 (C-9), 30.5 (C-10), 27.6* (br, C-7). (*) This signal was detected through HSQC/HMBC experiments.

Protonation of Li_2[1] with TfOH (NMR experiment). In an NMR tube, $Li_2[\mathbf{1}]$ (13 mg, 0.03 mmol) was dissolved in THF-d_8 (0.6 mL) to obtain a deep violet solution. One drop of neat TfOH was added via syringe at room temperature, whereupon the upper layer of the reaction solution immediately turned colorless. The initial deep violet color of the entire mixture was restored by slight agitation of the NMR tube.

An NMR spectroscopic (^{1}H, ^{11}B) investigation of the reaction mixture revealed Li[**1H**] as the major reaction product (see the SI for a plot of the ^{1}H NMR spectrum). We aimed at the addition of substoichiometric amounts of TfOH, and indeed, the ratio between the formed Li[**1H**] and the unreacted $Li_2[\mathbf{1}]$ is approximately 1:3. *Note*: We have also synthesized Li[**1H**] from **1** and Li[$HBEt_3$] on a preparative scale and isolated Li[**1H**] in pure form to obtain an authentic sample for comparison (see below).

Synthesis of Li[1]. THF (5 mL) was added with stirring at room temperature to a solid mixture of red, microcrystalline $Li_2[\mathbf{1}]$ × 0.7 C_7H_8 (46 mg, 0.094 mmol; the amount of C_7H_8 contained in the sample was estimated by ^{1}H NMR spectroscopy) and crystalline **1** (42 mg, 0.10 mmol). Within 1 min, both solids were completely dissolved to give a dark green solution. Stirring was continued for 1 h and all volatiles were removed in vacuo to obtain a dark green solid. Yield: 108 mg. Very dark green crystal blocks of $[Li(thf)_4][\mathbf{1}]$ × THF suitable for X-ray crystallography were grown by addition of Et_2O to a solution of Li[**1**] in THF until a precipitate formed. The precipitate was allowed to settle, the clear, saturated supernatant was decanted, and stored at −30 °C. Anal. Calcd for $C_{50}H_{68}B_2LiO_5$ (777.60): C, 77.23; H, 8.81; Found: C, 76.55; H, 8.67.

Synthesis of Li[1H]. A solution of Li[$HBEt_3$] in THF (1.0 M; 0.24 mL, 0.24 mmol) was added dropwise with stirring at room temperature via syringe to a yellow solution of **1** (100 mg, 0.24 mmol) in C_6H_6 (8 mL). The reaction mixture turned colorless and a colorless precipitate formed within 1 h. After the suspension had been stored at room temperature for 16 h without stirring, the supernatant was discarded and the colorless microcrystalline solid was briefly dried under vacuum. Yield: 142 mg (0.20 mmol, 83%). Colorless crystals of $[Li(thf)_4][\mathbf{1H}]$ suitable for X-ray crystallography were grown by recrystallization of this material from C_6H_6. *Note*: The molecular composition $[Li(thf)_4][\mathbf{1H}]$ was used to calculate the obtained yield. However, upon prolonged storage of the sample under a vacuum, the Li^+ ions gradually lose some of their thf ligands. According to ^{1}H NMR spectroscopy, exhaustively dried microcrystalline samples finally had a composition of approximately $[Li(thf)_2][\mathbf{1H}]$. ^{1}H NMR (500.2 MHz, THF-d_8, 298 K) δ = 8.09−8.05 (m, 2H; H-1a), 8.00−7.96 (m, 2H; H-1b), 7.57−7.49 (m, 4H; H-4a,4b), 7.03−6.96 (m, 8H; H-2a,2b,3a,3b), 2.00 (d, ^3J(H,H) = 7.0 Hz, 2H; H-8), 1.83* (n. r., 1H; BHB), 1.03 (dt, ^3J(H,H) = 7.0 Hz, 2.4 Hz, 1H; H-7), 0.58 (s, 9H; H-10); ^{1}H NMR (500.2 MHz, C_6D_6, 298 K) δ = 8.50 (m, 2H; H-1a), 8.38 (m, 2H; H-1b), 7.79 (m, 2H; H-4a), 7.76 (m, 2H; H-4b), 7.33−7.25 (m, 8H; H-2a,2b,3a,3b), 2.44 (d, ^3J(H,H) = 7.1 Hz, 2H; H-8), 2.03 (t, ^3J(H,H) = 7.1 Hz, 1H; H-7), 1.01 (s, 9H; H-10), n. o. (BHB); ^{11}B NMR (96.3 MHz, THF-d_8, 298 K) δ = −11.6 (n. r.; $h_{1/2}$ = 360 Hz); ^{11}B{^{1}H} NMR (96.3 MHz, THF-d_8, 298 K) δ = −11.6 ($h_{1/2}$ = 340 Hz); ^{13}C{^{1}H} NMR (125.8 MHz, THF-d_8, 298 K) δ = 159.6** (br, C-6b), 157.3** (br, C-6a), 150.6 (C-5a), 149.8 (C-5b), 133.4 (C-1a), 131.3 (C-1b), 125.0, 124.6, 124.4, 124.4 (C-2a,2b,3a,3b), 118.5, 118.3 (C-4a,4b), 44.2 (C-8), 32.8 (C-9), 30.0 (C-10), 14.2 (br, C-7). (*) This signal was clearly visible only upon ^{11}B decoupling; its chemical shift value was further confirmed by a cross peak in the ^{1}H,^{1}H−COSY (to CH_2CH) and in the ^{1}H,^{11}B-HSQC spectrum. (**) This signal was detected through HSQC/HMBC experiments.

DOI: 10.1021/jacs.5b01192
J. Am. Chem. Soc. 2015, 137, 3705−3714

Anal. Calcd for $C_{46}H_{61}B_2LiO_4$ (706.51): C, 78.20; H, 8.70; Found: C, 77.55; H, 8.60; MS (ESI): *m/z* (%): 411.6 (100) ([**1H**]$^-$).

Crystal Structure Determinations. Data were collected on a STOE IPDS II two-circle diffractometer with a Genix Microfocus tube with mirror optics using Mo Kα radiation (λ = 0.71073 Å). The data were scaled using the frame scaling procedure in the *X-AREA* program system.[38] The structures were solved by direct methods using the program *SHELXS*[39] and refined against F^2 with full-matrix least-squares techniques using the program *SHELXL-97*.[39] [Li(Et$_2$O)$_2$][Li(Et$_2$O)][**1**]: In one Et$_2$O molecule, two C atoms are disordered over two positions with a site occupation factor of 0.55(1) for each of the major occupied sites. In a second Et$_2$O molecule, all four C atoms are disordered over two positions with a site occupation factor of 0.516(6) for each of the major occupied sites. The disordered atoms were isotropically refined. The H atom bonded to C(1) was freely refined. [Li(thf)$_4$][**1**] × THF: In one thf molecule, one methylene group is disordered over two positions with a site occupation factor of 0.55(2) for the major occupied site. In two thf molecules, two methylene groups are disordered over two positions with a site occupation factor of 0.528(9) and 0.51(1), respectively, for the major occupied site. The disordered atoms were isotropically refined. [Li(thf)$_4$][**1H**]: In one thf molecule, one C atom is disordered over two positions with a site occupation factor of 0.57(3) for the major occupied site. In another thf molecule, one C atom is disordered over two positions with a site occupation factor of 0.61(4) for the major occupied site. In a third thf molecule, two C atoms are disordered over two positions with a site occupation factor of 0.57(1) for each of the major occupied sites. The disordered atoms were isotropically refined. Bond lengths and angles in the disordered thf molecules were restrained to the same values as those in the nondisordered thf molecule. Due to the absence of anomalous scatterers, the absolute structure could not be determined and Friedel pairs were merged. The H atom bridging B(1) and B(2) was found in the difference Fourier map and freely refined.

CCDC reference numbers: 1037135 ([Li(Et$_2$O)$_2$][Li(Et$_2$O)][**1**]), 1037136 ([Li(thf)$_4$][**1**] × THF), 1037134 ([Li(thf)$_4$][**1H**]).

Computational Details. DFT calculations were carried out with the Gaussian program package.[40] The PBE0[41−44] hybrid functional was used and combined with the D3BJ atom-pairwise dispersion correction with Becke-Johnson damping as devised by Grimme.[45,46] Geometry optimizations, harmonic frequency calculations and wave function analyses were computed under gas-phase conditions with the TZVP basis set.[47] All stationary points reported were characterized as minima by eigenvalue analysis of the diagonalized Hessians. Natural localized molecular orbitals (NLMOs) were generated with the natural bond orbital (NBO) program.[48] Topological analyses of the electron density according to Bader's quantum theory of atoms in molecules (QTAIM)[15,49] were carried out with the Multiwfn code.[50,51] In all QTAIM-related cases the Poincaré−Hopf relationship for a consistent set of critical points, $n_{ncp} - n_{bcp} + n_{rcp} - n_{ccp} = 1$, was fulfilled. To account for effects of solvents (tetrahydrofuran), a polarizable continuum model[52] within the COSMO[53] approach was employed for the evaluation of orbital energies, NMR shieldings, absorption spectra, and isotropic hyperfine coupling constants. UV−vis absorption spectra along with the corresponding natural transition orbitals (NTO)[54] were computed using the TD-DFT approach.[55] For the calculation of EPR properties,[56] the GIAO formalism[57−59] together with the EPR-III basis set[60] was used. Multireference configuration interaction (MRCI)[61] calculations for the small cyclopropane and diboracyclopropane model systems were performed with the Molpro program suite[62] in conjunction with the cc-pVTZ basis sets.[63] The preceding multiconfigurational self-consistent field (MCSCF)[64] wave functions were constructed from a set of six active orbitals comprising the three bonding and three antibonding σ-type molecular orbitals of the three-membered ring, i.e., CAS(6,6) type wave functions. Graphical representations of molecular geometries, isosurfaces, and AIM bond paths were produced with the POV-Ray[65] software.

■ ASSOCIATED CONTENT

Supporting Information

Plots of the ^{1}H and ^{13}C{^{1}H} NMR spectra of Li$_2$[**1**] and Li[**1H**]; plot of the ^{1}H NMR spectrum of protonated Li$_2$[**1**] (NMR experiment). Details of the X-ray crystal structure analyses of [Li(Et$_2$O)$_2$][Li(Et$_2$O)][**1**], [Li(thf)$_4$][**1**] × THF, and [Li(thf)$_4$][**1H**]. Cyclic voltammetric and spectroelectrochemical investigation of **1**. Details of the EPR spectroscopic measurement of in situ-generated Li[**1**] in THF solution. Details of quantum-chemical calculations. This material is available free of charge via the Internet at http://pubs.acs.org.

■ AUTHOR INFORMATION

Corresponding Authors

max.holthausen@chemie.uni-frankfurt.de
matthias.wagner@chemie.uni-frankfurt.de

Notes

The authors declare no competing financial interest.

■ ACKNOWLEDGMENTS

A.H. wishes to thank the Fonds der Chemischen Industrie for a Ph.D. grant. The authors are grateful to Professor Dietmar Stalke for helpful literature hints regarding problematic charge-density topology situations. Quantum-chemical calculations have been performed at the Center for Scientific Computing (CSC) Frankfurt on the FUCHS and LOEWE-CSC high-performance computer clusters. This work was supported by the Beilstein-Institut, Frankfurt (Main), Germany, within the research collaboration NanoBiC.

■ REFERENCES

(1) Hübner, A.; Diehl, A. M.; Diefenbach, M.; Endeward, B.; Bolte, M.; Lerner, H.-W.; Holthausen, M. C.; Wagner, M. *Angew. Chem., Int. Ed.* **2014**, *53*, 4832−4835. For an earlier example of an EPR-spectroscopically characterized B·B *1e2c* bond, see: Hoefelmeyer, J. D.; Gabbaï, F. P. *J. Am. Chem. Soc.* **2000**, *122*, 9054−9055.

(2) Hübner, A.; Diehl, A. M.; Bolte, M.; Lerner, H.-W.; Wagner, M. *Organometallics* **2013**, *32*, 6827−6833. The formation of B−B σ bonds has been suggested as result of the two-electron reduction of 1,8-diborylated naphthalenes during cyclic voltammetry: Melaïmi, M.; Solé, S.; Chiu, C.-W.; Wang, H.; Gabbaï, F. P. *Inorg. Chem.* **2006**, *45*, 8136−8143.

(3) Shoji, Y.; Matsuo, T.; Hashizume, D.; Gutmann, M. J.; Fueno, H.; Tanaka, K.; Tamao, K. *J. Am. Chem. Soc.* **2011**, *133*, 11058−11061.

(4) Grigsby, W. J.; Power, P. P. *J. Am. Chem. Soc.* **1996**, *118*, 7981−7988.

(5) Hübner, A.; Qu, Z.-W.; Englert, U.; Bolte, M.; Lerner, H.-W.; Holthausen, M. C.; Wagner, M. *J. Am. Chem. Soc.* **2011**, *133*, 4596−4609.

(6) In THF solution, the two-electron reduction of **1** proceeds much more rapidly and is complete within hours. We have confirmed the formation of Li$_2$[**1**] by NMR spectroscopy and by X-ray crystallography ([Li(thf)$_2$]$_2$[**1**] and [Li(thf)$_4$][Li(thf)$_2$][**1**]; in both cases, the poor crystal quality precludes publication of the data). However, the reaction in THF is less selective than in toluene, and in the case of the latter solvent, precipitation of Li$_2$[**1**] facilitates its isolation in pure form.

(7) Elschenbroich, C. *Organometallics*; Wiley-VCH: Weinheim, 2006.

(8) Nöth, H.; Wrackmeyer, B. Nuclear Magnetic Resonance Spectroscopy of Boron Compounds. In *NMR Basic Principles and Progress*; Diehl, P., Fluck, E., Kosfeld, R., Eds.; Springer: Berlin, 1978.

(9) (a) East, A. L. L.; Liu, Z. F.; McCague, C.; Cheng, K.; Tse, J. S. *J. Phys. Chem. A* **1998**, *102*, 10903−10911. (b) Takeuchi, T.; Shirai, Y.; Matsumura, Y.; Iwai, K.; Matsutani, T.; Oshita, J.; Naka, A. *Surf. Interface Anal.* **2006**, *38*, 1650−1653. (c) Watanabe, Y.; Maeda, S.;

DOI: 10.1021/jacs.5b01192
J. Am. Chem. Soc. 2015, 137, 3705−3714

Ohno, K. *Chem. Phys. Lett.* **2007**, *447*, 21−26. (d) Savoca, M.; Langer, J.; Dopfer, O. *Angew. Chem., Int. Ed.* **2013**, *52*, 1568−1571.
(10) (a) Rathke, M. W.; Kow, R. *J. Am. Chem. Soc.* **1972**, *94*, 6854−6856. (b) Matteson, D. S. *Synthesis* **1975**, 147−158. (c) Wilson, J. W. *J. Organomet. Chem.* **1980**, *186*, 297−300. (d) Matteson, D. S.; Moody, R. J. *Organometallics* **1982**, *1*, 20−28. (e) Power, P. P. *Chem. Rev.* **1999**, *99*, 3463−3503. (f) Yu, J.; Kehr, G.; Daniliuc, C. G.; Erker, G. *Eur. J. Inorg. Chem.* **2013**, 3312−3315.
(11) Carpenter, J. E.; Weinhold, F. *J. Mol. Struct.: THEOCHEM* **1988**, *46*, 41−62.
(12) Weinhold, F.; Landis, C. R. *Discovering Chemistry with Natural Bond Orbitals*; John Wiley & Sons: Hoboken, NJ, 2012.
(13) Landis, C. R.; Weinhold, F. The NBO View of Chemical Bonding. In *The Chemical Bond: Fundamental Aspects of Chemical Bonding*; Frenking, G., Shaik, S., Eds.; Wiley-VCH: Weinheim, 2014.
(14) Reed, A. E.; Schleyer, P. v. R. *J. Am. Chem. Soc.* **1990**, *112*, 1434−1445.
(15) Bader, R. F. W. *Atoms in Molecules: A Quantum Theory*; Oxford University Press: Oxford, 1994.
(16) Bader, R. F. W. *J. Phys. Chem. A* **2009**, *113*, 10391−10396.
(17) Bader, R. F. W. *J. Phys. Chem. A* **1998**, *102*, 7314−7323.
(18) Matta, C. F.; Hernández-Trujillo, J.; Tang, T.-H.; Bader, R. F. W. *Chem.—Eur. J.* **2003**, *9*, 1940−1951.
(19) Bader, R. F. W.; Fang, D.-C. *J. Chem. Theory Comput.* **2005**, *1*, 403−414.
(20) Bader, R. F. W. *Chem.—Eur. J.* **2006**, *12*, 7769−7772.
(21) Bader, R. F. W. *Chem.—Eur. J.* **2006**, *12*, 2896−2901.
(22) Poater, J.; Solà, M.; Bickelhaupt, F. M. *Chem.—Eur. J.* **2006**, *12*, 2889−2895.
(23) Poater, J.; Solà, M.; Bickelhaupt, F. M. *Chem.—Eur. J.* **2006**, *12*, 2902−2905.
(24) Weinhold, F.; Schleyer, P. v. R.; McKee, W. C. *J. Comput. Chem.* **2014**, *35*, 1499−1508.
(25) Macchi, P.; Garlaschelli, L.; Sironi, A. *J. Am. Chem. Soc.* **2002**, *124*, 14173−14184.
(26) Macchi, P.; Sironi, A. *Coord. Chem. Rev.* **2003**, *238*, 383−412.
(27) Farrugia, L. J.; Evans, C.; Tegel, M. *J. Phys. Chem. A* **2006**, *110*, 7952−7961.
(28) Henn, J.; Leusser, D.; Stalke, D. *J. Comput. Chem.* **2007**, *28*, 2317−2324.
(29) Flierler, U.; Burzler, M.; Leusser, D.; Henn, J.; Ott, H.; Braunschweig, H.; Stalke, D. *Angew. Chem., Int. Ed.* **2008**, *47*, 4321−4325.
(30) Farrugia, L. J.; Evans, C.; Lentz, D.; Roemer, M. *J. Am. Chem. Soc.* **2009**, *131*, 1251−1268.
(31) Mousavi, M.; Frenking, G. *Organometallics* **2013**, *32*, 1743−1751.
(32) Mousavi, M.; Frenking, G. *J. Organomet. Chem.* **2013**, *748*, 2−7.
(33) Jacobsen, H. *J. Comput. Chem.* **2009**, *30*, 1093−1102.
(34) Götz, K.; Kaupp, M.; Braunschweig, H.; Stalke, D. *Chem.—Eur. J.* **2009**, *15*, 623−632.
(35) We note in passing that a QTAIM analysis performed on a charge density obtained from a MRCISD/cc-pVTZ single point calculation on the PBE0D/TZVP minimum structure resulted in essentially identical results, which validates again the suitability of the chosen DFT approach.
(36) See chapter 4 in ref 15.
(37) Foroutan-Nejad, C.; Shahbazian, S.; Marek, R. *Chem.—Eur. J.* **2014**, *20*, 10140−10152.
(38) *X-AREA: Diffractometer Control Program System*; Stoe & Cie: Darmstadt, Germany, 2002.
(39) Sheldrick, G. M. *Acta Crystallogr., Sect. A: Found. Crystallogr.* **2008**, *64*, 112−122.
(40) Frisch, M. J.; Trucks, G. W.; Schlegel, H. B.; Scuseria, G. E.; Robb, M. A.; Cheeseman, J. R.; Scalmani, G.; Barone, V.; Mennucci, B.; Petersson, G. A.; Nakatsuji, H.; Caricato, M.; Li, X.; Hratchian, H. P.; Izmaylov, A. F.; Bloino, J.; Zheng, G.; Sonnenberg, J. L.; Hada, M.; Ehara, M.; Toyota, K.; Fukuda, R.; Hasegawa, J.; Ishida, M.; Nakajima, T.; Honda, Y.; Kitao, O.; Nakai, H.; Vreven, T.; Montgomery, J. A., Jr.; Peralta, J. E.; Ogliaro, F.; Bearpark, M.; Heyd, J. J.; Brothers, E.; Kudin, K. N.; Staroverov, V. N.; Kobayashi, R.; Normand, J.; Raghavachari, K.; Rendell, A.; Burant, J. C.; Iyengar, S. S.; Tomasi, J.; Cossi, M.; Rega, N.; Millam, J. M.; Klene, M.; Knox, J. E.; Cross, J. B.; Bakken, V.; Adamo, C.; Jaramillo, J.; Gomperts, R.; Stratmann, R. E.; Yazyev, O.; Austin, A. J.; Cammi, R.; Pomelli, C.; Ochterski, J. W.; Martin, R. L.; Morokuma, K.; Zakrzewski, V. G.; Voth, G. A.; Salvador, P.; Dannenberg, J. J.; Dapprich, S.; Daniels, A. D.; Farkas, Ö.; Foresman, J. B.; Ortiz, J. V.; Cioslowski, J.; Fox, D. J. *Gaussian 09*, Revision D.01; Gaussian, Inc.: Wallingford, CT, 2013; http://www.gaussian.com.
(41) Perdew, J. P.; Burke, K.; Ernzerhof, M. *Phys. Rev. Lett.* **1996**, *77*, 3865−3868.
(42) Perdew, J. P.; Burke, K.; Ernzerhof, M. *Phys. Rev. Lett.* **1997**, *78*, 1396−1396.
(43) Perdew, J. P.; Ernzerhof, M.; Burke, K. *J. Chem. Phys.* **1996**, *105*, 9982−9985.
(44) Adamo, C.; Barone, V. *J. Chem. Phys.* **1999**, *110*, 6158−6170.
(45) Goerigk, L.; Grimme, S. *J. Chem. Theory Comput.* **2011**, *7*, 291−309.
(46) Grimme, S.; Ehrlich, S.; Goerigk, L. *J. Comput. Chem.* **2011**, *32*, 1456−1465.
(47) Schäfer, A.; Huber, C.; Ahlrichs, R. *J. Chem. Phys.* **1994**, *100*, 5829−5835.
(48) Glendening, E. D.; Landis, C. R.; Weinhold, F. *Wiley Interdiscip. Rev.: Comput. Mol. Sci.* **2012**, *2*, 1−42.
(49) Matta, C. F., Boyd, R. J., Eds.; *The Quantum Theory of Atoms in Molecules*; Wiley-VCH: Weinheim, 2007.
(50) Lu, T. *Multiwfn 3.2.1—A Multifunctional Wavefunction Analyzer*; School of Chemical and Biological Engineering, University of Science and Technology: Beijing, China, 2013; http://multiwfn.codeplex.com.
(51) Lu, T.; Chen, F. *J. Comput. Chem.* **2012**, *33*, 580−592.
(52) Tomasi, J.; Mennucci, B.; Cammi, R. *Chem. Rev.* **2005**, *105*, 2999−3094.
(53) Klamt, A. *Wiley Interdiscip. Rev.: Comput. Mol. Sci.* **2011**, *1*, 699−709.
(54) Martin, R. L. *J. Chem. Phys.* **2003**, *118*, 4775−4777.
(55) Scalmani, G.; Frisch, M. J.; Mennucci, B.; Tomasi, J.; Cammi, R.; Barone, V. *J. Chem. Phys.* **2006**, *124* (094107), 1−15.
(56) Ciofini, I.; Adamo, C.; Barone, V. *J. Chem. Phys.* **2004**, *121*, 6710−6718.
(57) Ditchfield, R. *Mol. Phys.* **1974**, *27*, 789−807.
(58) Wolinski, K.; Hinton, J. F.; Pulay, P. *J. Am. Chem. Soc.* **1990**, *112*, 8251−8260.
(59) Cheeseman, J. R.; Trucks, G. W.; Keith, T. A.; Frisch, M. J. *J. Chem. Phys.* **1996**, *104*, 5497−5509.
(60) Barone, V. Structure, Magnetic Properties and Reactivities of Open-Shell Species from Density Functional and Self-Consistent Hybrid Methods. In *Recent Advances in Density Functional Methods*; World Scientific: Singapore, 1995; Vol. *1*, pp 287−334.
(61) Werner, H.-J.; Knowles, P. J. *J. Chem. Phys.* **1988**, *89*, 5803−5814.
(62) Werner, H.-J.; Knowles, P. J.; Knizia, G.; Manby, F. R.; Schütz, M.; Celani, P.; Korona, T.; Lindh, R.; Mitrushenkov, A.; Rauhut, G.; Shamasundar, K. R.; Adler, T. B.; Amos, R. D.; Bernhardsson, A.; Berning, A.; Cooper, D. L.; Deegan, M. J. O.; Dobbyn, A. J.; Eckert, F.; Goll, E.; Hampel, C.; Hesselmann, A.; Hetzer, G.; Hrenar, T.; Jansen, G.; Köppl, C.; Liu, Y.; Lloyd, A. W.; Mata, R. A.; May, A. J.; McNicholas, S. J.; Meyer, W.; Mura, M. E.; Nicklaß, A.; O'Neill, D. P.; Palmieri, P.; Peng, D.; Pflüger, K.; Pitzer, R.; Reiher, M.; Shiozaki, T.; Stoll, H.; Stone, A. J.; Tarroni, R.; Thorsteinsson, T.; Wang, M. *MOLPRO*, Version 2012.1; University College Cardiff Consultants Ltd.: Cardiff, U.K., 2012; http://www.molpro.net.
(63) Dunning, T. H. *J. Chem. Phys.* **1989**, *90*, 1007−1023.
(64) Werner, H.-J.; Knowles, P. J. *J. Chem. Phys.* **1985**, *82*, 5053−5063.
(65) *Persistence of Vision Raytracer*, Version 3.6; Persistence of Vision Pty. Ltd.: Williamstown, Victoria, Australia, 2004; http://www.povray.org.

DOI: 10.1021/jacs.5b01192
J. Am. Chem. Soc. 2015, 137, 3705−3714